

CFD Analysis For Assessing The Effect Of Wind On The Thermal Control Of The Mars Science Laboratory Curiosity Rover

Pradeep Bhandari¹ and Kevin Anderson^{2,3}

Jet Propulsion Laboratory, California Institute of Technology, Pasadena, CA, 91740

The challenging range of landing sites for which the Mars Science Laboratory Rover was designed, requires a rover thermal management system that is capable of keeping temperatures controlled across a wide variety of environmental conditions. On the Martian surface where temperatures can be as cold as -123°C and as warm as 38°C , the rover relies upon a Mechanically Pumped Fluid Loop (MPFL) Rover Heat Rejection System (RHRS) and external radiators to maintain the temperature of sensitive electronics and science instruments within a -40°C to 50°C range. The RHRS harnesses some of the waste heat generated from the rover power source, known as the Multi Mission Radioisotope Thermoelectric Generator (MMRTG), for use as survival heat for the rover during cold conditions. The MMRTG produces 110 W of electrical power while generating waste heat equivalent to approximately 2000 W. Heat exchanger plates (hot plates) positioned close to the MMRTG pick up this survival heat from it by radiative heat transfer. Winds on Mars can be as fast as 15 m/s for extended periods. They can lead to significant heat loss from the MMRTG and the hot plates due to convective heat pick up from these surfaces. Estimation of this convective heat loss cannot be accurately and adequately achieved by simple textbook based calculations because of the very complicated flow fields around these surfaces, which are a function of wind direction and speed. Accurate calculations necessitated the employment of sophisticated Computational Fluid Dynamics (CFD) computer codes. This paper describes the methodology and results of these CFD calculations. Additionally, these results are compared to simple textbook based calculations that served as benchmarks and sanity checks for them. And finally, the overall RHRS system performance predictions will be shared to show how these results affected the overall rover thermal performance.

Nomenclature

<i>AFT</i>	=	<i>Allowable Flight Temperature</i>
<i>B.C.</i>	=	<i>Boundary Condition</i>
<i>BOL</i>	=	<i>Beginning of Life</i>
<i>CFC-11</i>	=	<i>Trichloromonofluoromethane (Refrigerant 11)</i>
<i>CFD</i>	=	<i>Computational Fluid Dynamics</i>
<i>CIPA</i>	=	<i>Cruise Integrated Pump Assembly</i>
<i>CHRS</i>	=	<i>Cruise Heat Rejection System</i>
<i>EDL</i>	=	<i>Entry, Descent and Landing</i>
<i>HRS</i>	=	<i>Heat Rejection System</i>
<i>HXCH</i>	=	<i>Heat Exchanger</i>
<i>I.C.</i>	=	<i>Initial Condition</i>
<i>JPL</i>	=	<i>Jet Propulsion Laboratory</i>
<i>MER</i>	=	<i>Mars Exploration Rover</i>

¹ Principal Engineer, Propulsion, Thermal & Materials Engineering Section, 4800 Oak Grove Drive, Pasadena, CA-91740, M/S 125-123, AIAA Member

² Senior Engineer, Propulsion, Thermal & Materials Engineering Section, 4800 Oak Grove Drive, Pasadena, CA-91740, M/S 125-123, AIAA Member

³ Professor of Mechanical Engineering, California State Polytechnic University, 3801 West Temple Ave, Pomona, CA-91768, Building 17-2353, AIAA Member

MMRTG = *Multi Mission Radioisotope Thermoelectric Generator*
MPF = *Mars Pathfinder*
MPFL = *Mechanically Pumped Fluid Loop*
MSL = *Mars Science Laboratory*
NASA = *National Aeronautics and Space Administration*
RAMP = *Rover Avionics Mounting Plate*
RIPA = *Rover Integrated Pump Assembly*
RHRS = *Rover Heat Rejection System*
WCC = *Worst Case Cold*
WCH = *Worst Case Hot*
V&V = *Verification and Validation*

I. Introduction

THE MSL mission, with its Curiosity rover currently on Mars, follows the general design paradigm of the previous JPL rover missions to Mars (Mars Pathfinder, MPF^{1,2,3,4,5} and Mars Exploration Rovers, MER^{6,7}). The external configuration of the MSL spacecraft looks similar to that of MPF and MER. At 4.5 m, the diameter of the MSL⁸ spacecraft is almost twice that of the MPF and MER spacecraft (2.6 m). MSL features a rover enclosed in an aero-shell for protection during entry and descent onto the planet's surface. A cruise stage carries the lander and aero-shell enclosure from Earth to Mars and will separate from the Lander, just prior to Entry, Descent and Landing (EDL). Figure 1 shows a rendering of the rover packed into the aero-shell enclosure with the cruise stage attached at the top. MSL landed on Mars on Aug 5th, 2012 and has operated successfully since then.

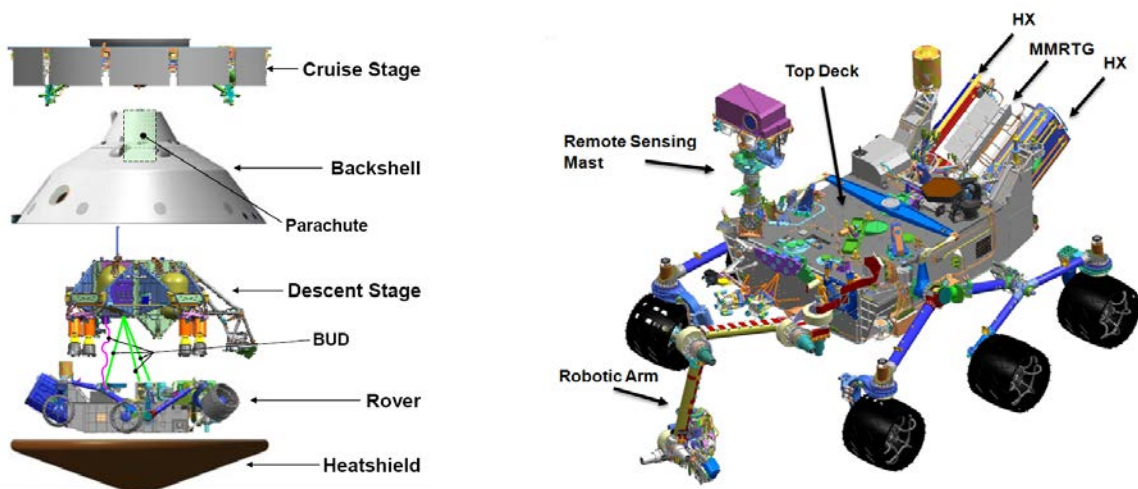


Figure 1. MSL Spacecraft and Deployed Rover.

The Multi Mission Radioisotope Thermoelectric Generator (MMRTG) is structurally attached to the rover and dissipates 2000 W of waste heat and weighs about 40 kg. The descent stage, containing the descent propulsion system and avionics, is adjacent to the stowed rover. The cruise stage contains the avionics, cruise propulsion system and the pumped loop radiators.

II. Overall MSL Thermal Architecture

The MSL spacecraft and the rover utilize mechanically pumped single phase fluid loop heat rejection systems (HRS) to create the backbone for thermal control of both systems: the Cruise Heat Rejection System (CHRS) and Rover Heat Rejection System (RHRS). Both fluid loops use Refrigerant-11 (CFC-11) as the working fluid. Figure 2 shows the overall thermal architecture.

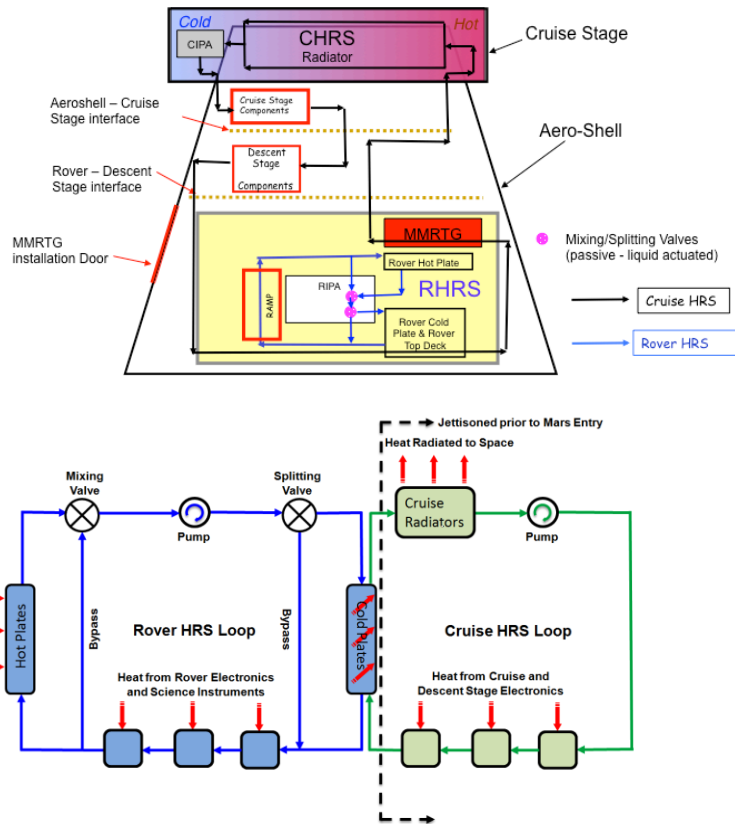


Figure 2. Schematics of Two HRS Fluid Loops.

The CHRS operates during the cruise portion of the MSL mission, from pre-launch to about an hour prior to the entry into the Mars environment. Its main function is to remove the waste heat from the MMRTG while maintaining its temperatures in a benign range (~100 to 180°C). It also picks up dissipated heat from the equipment on the rover and on the cruise/descent stages of the MSL spacecraft. Aluminum tubing is primarily employed in the loop, with a fraction being stainless steel.

Just prior to EDL, the working fluid in the CHRS loop is vented and the cruise stage containing the CHRS pumps is separated from the lander. Since EDL is short-lived (20 minutes) the thermal mass of the MMRTG prevents it from overheating, in spite of the lack of cooling of the MMRTG during this phase.

For the rover, the overall system approach is to utilize a single-phase mechanically pumped fluid loop based HRS for the majority of the thermal control of the rover during Mars surface operations. The main impetus behind this is to utilize, as much as possible, the waste heat from the MMRTG to provide heat to the rover for cold conditions as well to use the RHRS to reject heat from the rover to external radiators during hot conditions.

The combination of the MMRTG waste heat and the fluid loop greatly simplifies the rover thermal design in terms of the level of thermal isolation required to maintain the rover and payload at allowable temperatures during cold conditions. It also greatly improves the robustness of the design, decouples the mechanical design and configuration from the thermal design and reduces the level of testing required. The references^{8,9,10,11,12,13,15} provide a brief history of HRS loops, particularly from JPL's experience in using them for Mars missions.

Figure 3 has the schematic of the fluid loop of the RHRS. Both the Rover Integrated Pump Assembly (RIPA) as well as the Cruise Integrated Pump Assembly (CIPA) have two pumps each for the sake of redundancy. However, only one pump is powered at any time. There is also a metal bellows accumulator to accommodate volume changes due to temperature changes and small leaks in the system during the mission. A simplified schematic of the RIPA is shown within Fig. 3. Each of the two pumps has its own electronics to power it independently. The input power for RIPA (including the electronics) is 10 W. Each pump and thermal control valve subassembly has check valves upstream and downstream of them to ensure no recirculation flow occurs when one pump is idle and the other is running. The filters protect the pump bearings from particles in the flow stream. Each filter has a check valve in

parallel to allow the flow to continue (although without providing protection for the pumps) in the event of a filter saturating or clogging. More detailed description of the two HRSs can be found in references 8-14.

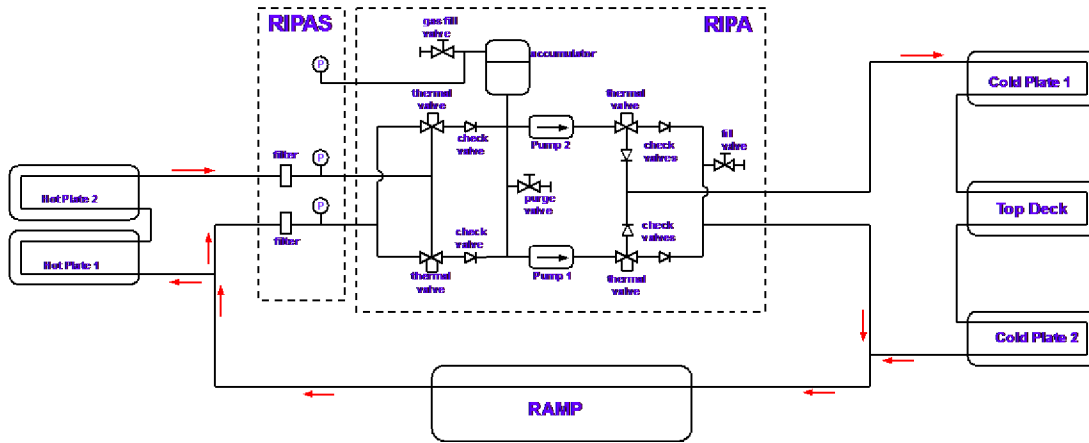


Figure 3. RHRs Schematic.

III. Winds on Mars

The Martian atmosphere is predominantly composed of Carbon Dioxide (CO_2) gas with a pressure of about 1000 Pa (8 Torr). A plot of the wind speeds observed by the Viking 2 mission to Mars is shown in Fig. 4. The 90th percentile maximum sustained wind speed is 15 m/s and it was used to design the rover. Transient gusts can be higher than this value but are short lived. The time constant of the thermal system would be able to handle these intermittent excursions from the design point.

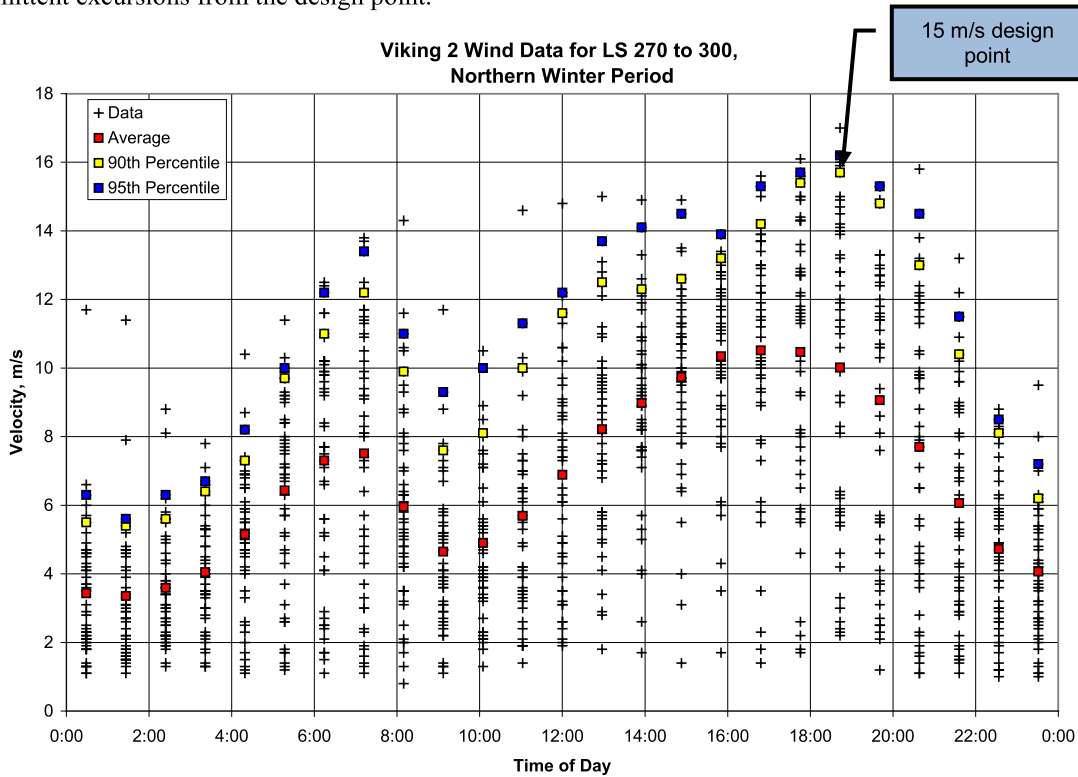


Figure 4. Martian Wind Speeds

IV. Effect of Martian Wind on the MMRTG and its Heat Exchangers

The CHRS interface with the rover occurs on the two MMRTG Heat Exchanger plates¹⁴ (Fig. 5 and 6), which flank the sides of the MMRTG. Each of the two heat exchanger plates are composed of a hot plate and a cold plate pair that have the HRS tubing epoxied on them. The purpose of these hot plates (inside surface of heat exchanger plates) is to capture radiative waste heat from the MMRTG during the surface phase of the mission and use it to warm the rover internals with the help of the HRS fluid flow. The purpose of the cold plates (outside surfaces of the heat exchanger plates) is to serve as radiators for the heat from the rover electronics/instruments. The hot and cold plates are mechanically attached to each other via a honeycomb composite structure that minimizes the thermal coupling between the two to reduce the crosstalk between their totally different functions.

The function of the Rover HRS is to transfer heat from the rover to the cold plates on the MMRTG Heat Exchangers or to pick up waste heat (radiatively) from the hot MMRTG and transfer it to the rover. During the cruise phase of the mission, the RHRS loop moves waste heat from the inside of the rover to these cold plates. A tube-to-tube counter flow heat exchanger between the Cruise and Rover HRS is attached to the cold plates of the MMRTG heat exchanger and serves to pick up heat from the Rover HRS and transfer it to the Cruise HRS.

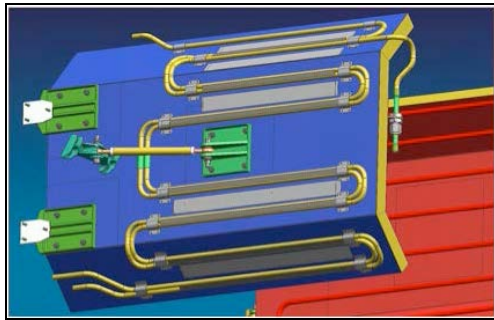


Figure 5. Rover Heat Exchanger Cold Plate

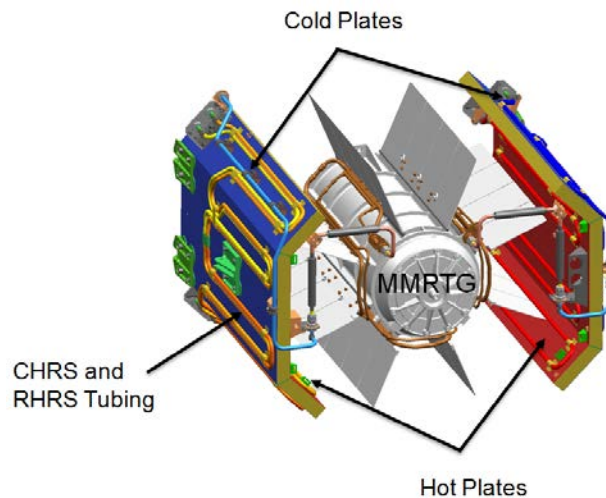


Figure 6. RHRS Heat Exchanger Assemblies, Red Face sheets-Hot Plates, Blue Face sheets-Cold Plates

The size of the HXCH plates is determined by the tradeoff between the hot and cold cases – make them too large and then they would pick up too much heat from the MMRTG (also the MMRTG would be warmer due to their view blockage). This would be a problem in the hot case because this unneeded excess collected heat would then have to be rejected by the real estate starved RHRS radiators (HXCH cold plates and rover top deck). So the HXCH is optimized to be able to meet both the hottest and coldest operating conditions. Martian atmospheric wind is always colder than the MMRTG and in most cases colder than the HXCH hot plates. Hence it would tend to remove some of the waste heat available from the MMRTG as well as from the hot plates. So for a given geometric configuration of HXCH and MMRTG, they would both be colder in the presence of wind. Since one of the primary jobs of the RHRS is to pick up waste heat from the MMRTG in the cold conditions, this heat removed by the wind would make less of the waste heat available from the MMRTG to be used in the rover thermal control. Hence an accurate accounting of the thermal effect of the wind is very important to understand and design the RHRS to ascertain its adequacy in the coldest conditions.

Since Martian wind can impinge on the MMRTG and its HXCH from any direction, lacking a windbreaker, the direction of the wind along the MMRTG axis would clearly have the most deleterious effect, as seen in Fig. 7. Wind in other directions would encounter natural windbreakers in the form of the rover chassis itself (for wind along the MMRTG axis but coming from the opposite direction) and the HXCH plates (for wind in direction perpendicular to the MMRTG axis). So the most obvious windbreaker location is where it bridges the HXCH plates on the anti-rover side of the MMRTG.

In spite of the obvious improvement of the heat pick up from the MMRTG due to the windbreaker, the actual effect of the wind is quite complicated due to the 3-D flow around the complex geometries of the MMRTG, HXCH plates, rover chassis and the windbreaker. Some finite wind speeds would be present past the windbreaker and the

HXCH plates in the vicinity of the MMRTG. These residual winds would lead to heat transfer coefficients higher than for natural convection, and would lead to some heat loss increases from the MMRTG and the HXCH hot plates (when compared to no wind). A heat transfer coefficient map is thus required by fluid/thermal modeling to make a correct heat balance on these surfaces. The cold plates do not get affected to any significant degree due to the wind because the RHRS fluid flow essentially almost completely bypasses the cold plate radiators to conserve the collected heat.

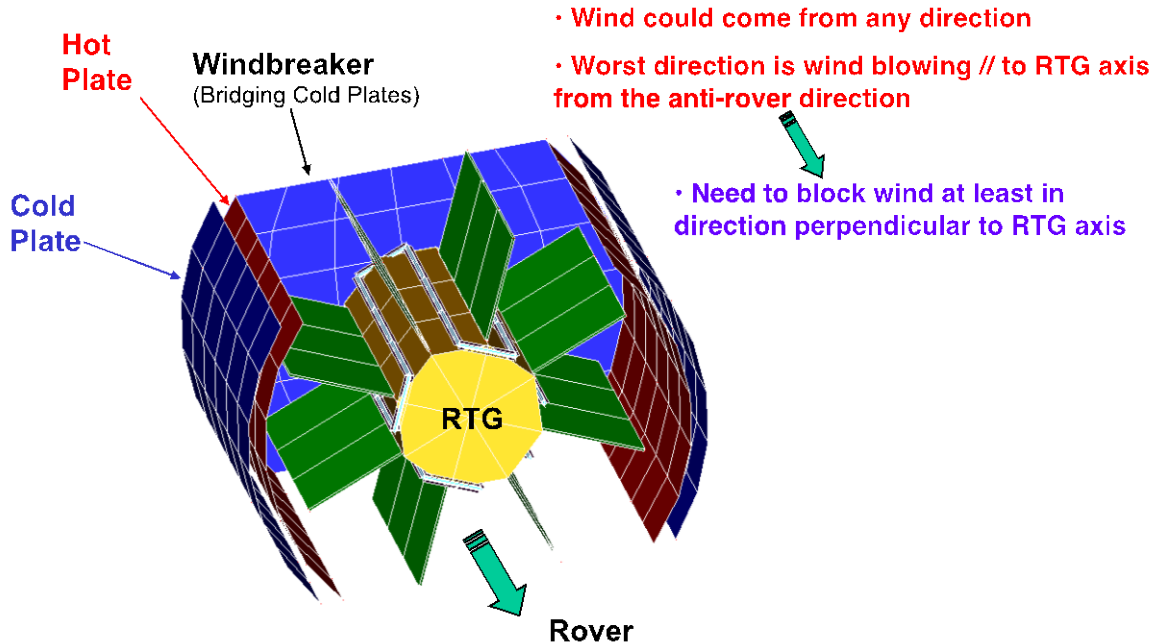


Figure 7. Windbreaker Functionality

V. CFD Analyses of the Effect of Winds on the MMRTG/HXCH heat losses

The CFD task was constrained by the overall thermal requirements placed on the project as well as by time and budget demands. As is typical with CFD analysis, several computer simulations were required in order to optimize the flow geometry. Subsequently several more “production” simulations were needed in order to exercise the model across the trade space of the given problem’s parameter ranges. This section of the paper focuses on the details of the CFD modeling process and documents the growth of the analysis as it reached maturity. The results of CFD provide valuable flow-field visualization feedback on the validity of a proposed flow-tailoring geometry design. In addition, CFD analysis bridges the gap between handbook correlations for the convective film coefficient “h-value”, which can be off by as much as 25% per Incropera and Dewitt¹⁶. From first-hand experience, the authors of this paper have witnessed uncertainties in theoretical convective film coefficient values up to 50%, especially when dealing with two-phase flows and/or modeling heat pipe thermo-physics. To this end, CFD is a valuable tool in the prediction of the h-value for convection dominated flow problems. These h-values derived from CFD can then later be used in system level models of the overall hardware in order to correlate the thermal model to actual on-station predictions. In closing, CFD can be used to mitigate some of the risks associated with determining the convective film coefficient for a given subsystem, and should only be used as a design guide. In all situations, an engineering unit level test is highly recommended in order to fully characterize and understand the h-values for a given piece of hardware. For this particular application, the CFD simulation data is used to gain quantitative understanding of the MMRTG/HXCH flow field physics while on operation in the Martian environment. The CFD data is used to derive heat transfer coefficients and provide a guide before engaging in thermal vacuum testing at the spacecraft hardware integration level. To this end, in order to properly understand the outputs of the CFD model, the CFD predictions must be compared to handbook correlations in order to place an uncertainty band on the CFD results. For complicated geometries this type of CFD model validation and verification (V&V) is paramount before one can accurately use the CFD predictions to guide thermal control system design work. Thus a series of V&V studies on simple geometries is carried out in unison with the modeling of the sophisticated flight hardware in order to place an error bar on the CFD predictions.

The CFD code used was Blue Ridge Numeric's CFDesign 2012. This code is a finite element based CFD fluid flow and heat transfer solver. The equations of motion being solved are the full Navier-Stokes with Conservation of Energy, Conjugate Heat Transfer, and the k-ε turbulent closure model. The CFDesign code employs the Galerkin Finite Element Method with pressure correction via the Semi-Implicit-Method for Pressure-Linked-Equations (SIMPLE) algorithm of Patankar¹⁷ to formulate and solve the equations of motion. The modeling flow path per Anderson et al.¹⁸ was used as follows:

1. Read in CAD geometry into CFDesign as Parasolid file
2. Create material data blocks
3. Assign B.C.'s / I.C.'s
4. Mesh using CFDESIGN's auto-mesher and tetrahedral elements, adjust y+ to control boundary layer physics
5. Solve x, y, z momentum equations
6. Solve pressure correction equation
7. Correct velocities via pressure correction based on the SIMPLE algorithm of Patankar³
8. Solve energy equation
9. Solve Turbulent Kinetic Energy equation
10. Solve Turbulent Kinetic Energy dissipation equation
11. Check convergence (go to 5)
12. Perform post-processing, i.e. plot h-values, temperature contours, velocity contours, etc.

The thermo-physical materials used for the working fluid medium of Carbon Dioxide gas (CO₂) were taken from the National Institute of Standards and Technology (NIST) database computer program NIST12¹⁹. The software program NIST12 allows users build a database of thermo physical properties as a function of temperature and pressure. For this project, the version of CFDesign used did not have CO₂ as a default material. Thus NIST12 was used to generate look-up tables in the form of polynomial curve fits for the density, thermal conductivity, specific heat, and viscosity of the CO₂. Curve fits used for the CO₂ properties are shown below in Fig. 8 through Fig. 12. Modeling inputs to the CFD software included specification of the Martian gravity vector, having a magnitude of 3.94 m/s² (40% of Earth's gravity), ambient pressure of 8 Torr (0.0105263158 atm), specific gas constant for the CO₂, R = 188.92 kJ/kg -K, and ambient temperature of CO₂ of 148.15 K. Thus, the NIST12 database used to build the curve fits of CO₂ were obtained for a pressure of 8 Torr.

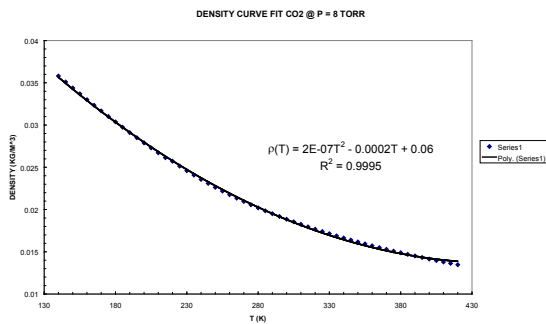


Figure 8. CO₂ Density Curve Fit from NIST12

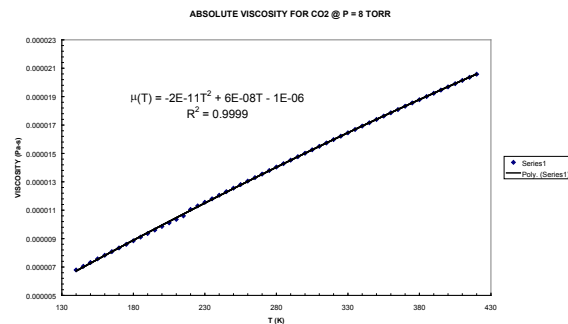


Figure 9. CO₂ Viscosity Curve Fit from NIST12

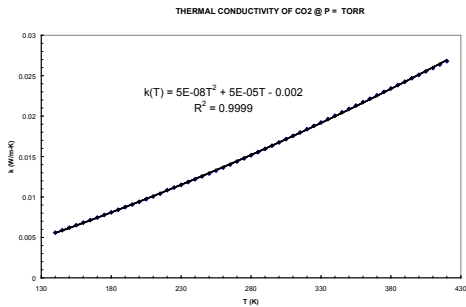


Figure 10. CO₂ Thermal Conductivity Curve Fit from NIST12

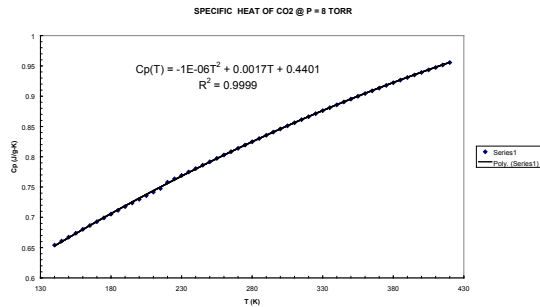


Figure 11. CO₂ Heat Capacity Curve Fit from NIST12

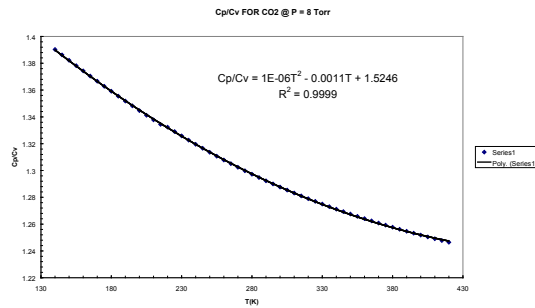


Figure 12. CO₂ Specific Heat Ratio Curve Fit from NIST12

In order to use the CFD software, it was first required to verify that the CO₂ was operating as a Newtonian Gas in the realm of operation and computer simulations. To this end, the Knudsen number, Kn, was computed. The Knudsen number is a non-dimensional parameter which ratios the mean free path of a molecule to its characteristic Newtonian flow length scale. For $0 < Kn < 0.1$, Navier-Stokes (continuum) flow is valid. Using 8 Torr CO₂ and the characteristic fluid dynamical length scale as that of the MMRTG fin thickness, $Kn \sim 10^{-7}$, continuum flow is valid and the Navier-Stokes governing equations solved within CFDesign are seen to hold for the modeling effort herein.

Before proceeding with the production CFD runs, a series of code V&V computer runs were carried out on simpler and easy to understand geometries. Figure 13 shows the set-up for a vertical plate in cross-flow. The plate solid mesh is in the presence of the fluid mesh with velocity vectors and velocity magnitude contours. The scale on the color bar ranges from 0 = blue to 16.1184 m/s = red.

The inputs for this validation case included: a flow speed of 10 m/s, ambient working fluid of air at 423.15 K, a 0.5 m by 0.5 m by 0.01 m thick aluminum plate held at 323.15 K. The external domain was a 2 m³ mesh with tetrahedral plate elements on the order of 0.01 m, and the domain element size of 0.2 m. This model contained approximately 50,000 fluid nodes, and 7000 nodes, for a total of 57,000 degrees of freedom. When comparing the convective film heat transfer coefficient (h-value) from the CFD model to that from the handbook, there is a 12.5% error, with the CFD h-value being 13% lower than the handbook h-value. This is to be expected, since the handbook correlation carries at least 25% uncertainty due to its underlying assumptions. Thus, the agreement of 12.5% is deemed acceptable for our application. Next, the plate of Fig. 13 was simulated with 8 Torr CO₂, and the error between CFD and theoretical h-values became 18%.

The next validation case performed was for the flow over a cylinder. Figure 14 shows the cylinder solid mesh and the fluid mesh, with streamlines and contours of velocity magnitude. The scale on the color bar ranges from 0 = blue to 15.4 m/s = red. For this airflow at 1 atm over the cylinder, agreement between CFD and theoretical h-values was 16%. When this simulation was run with 8 Torr CO₂, the error between CFD and theory was 25%. This large error is due to the realm of pressures at which the simulation was run. While still Newtonian, the effects of reduced pressure on the thermo-physical properties becomes more pronounced as the pressure is reduced. Again, this uncertainty of 25% is accounted for in the assumptions of the handbook correlation.

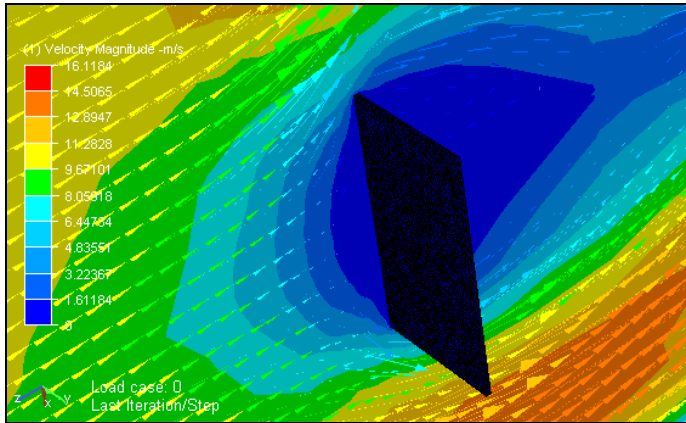


Figure 13. CFD Verification and Validation Case for Vertical Plate in Cross flow

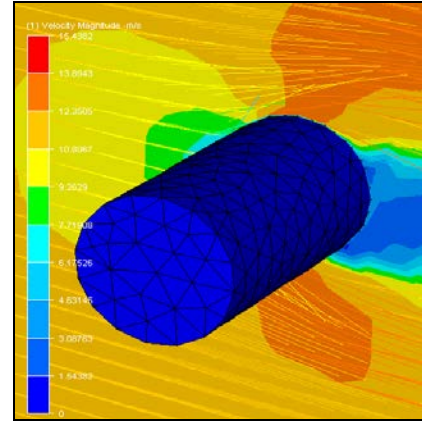


Figure 14. CFD Verification and Validation Case for Cylinder in Cross flow

Having completed the V&V CFD code test simulations, attention was focused on performing the analysis of the various windbreaker configurations proposed for the rover MMRTG/HXCH system. The boundary conditions for this series of simulations included an assumed ground temperature on Mars of 148.15 K, a rover exterior electronics box temperature of 173.15 K and various Martian wind speed magnitudes varying from 5, 10, 15, 20 m/s. The CFD model set-up for the MMRTG/HXCH hardware is shown below in Fig. 15.

The simulation employed incompressible CO₂ flow, with conjugate heat transfer (including radiation) and the standard k-ε turbulence model with 2000 W generated by the MMRTG, and 200 W removed from each heat exchanger (HXCH). It used 93,000 fluid elements and 13,000 solid elements for a total of 106,000 elements. Typical results of velocity vectors and magnitude from this simulation are shown in Fig. 16. The scale on the color bar ranges from 0 = blue to 20.3 m/s = red. Apparent are the areas of vortex shedding which develop at the leading edge of the HXCH plate. It was determined early on in the process of post-processing that a mapping of the heat transfer coefficients in the vicinity of the MMRTG, the fins, and the heat exchangers would be beneficial for performing quick analysis of the thermal control system design.

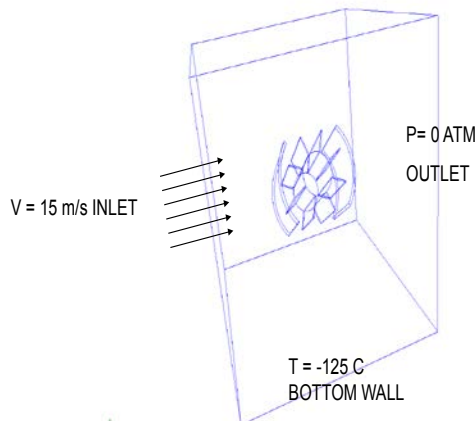


Figure 15. CFD Model Set-up for MMRTG/HXCH in Cross flow

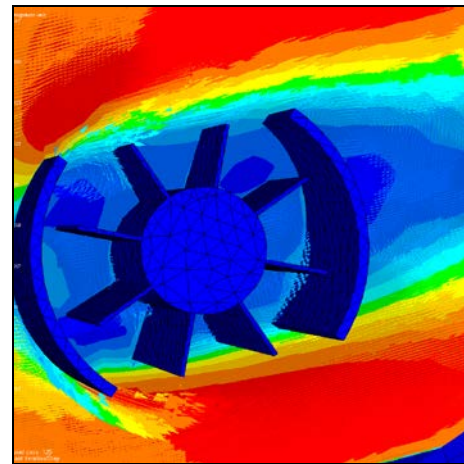


Figure 16. MMRTG/HXCH in Cross flow Velocity Vectors

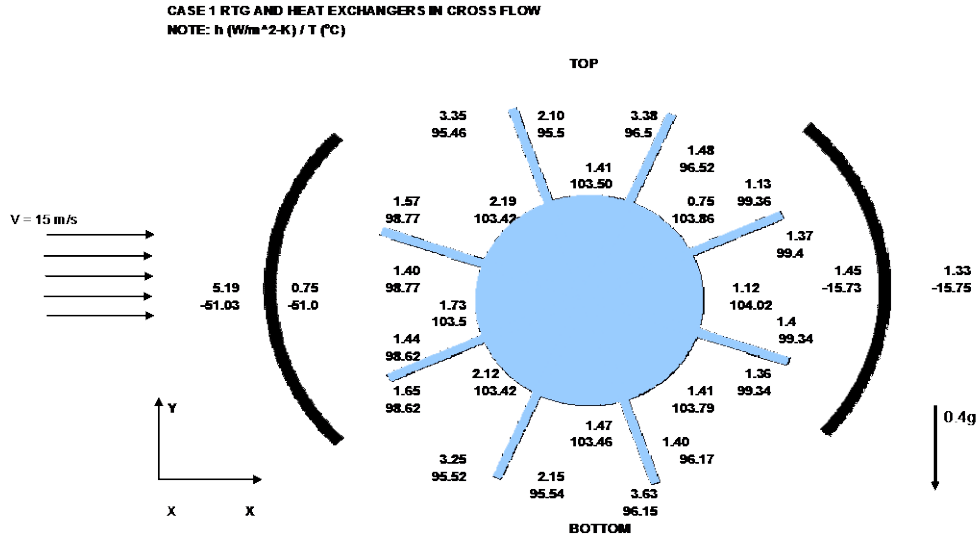


Figure 17. Post-Processing MMRTG/HXCH in Heat Transfer Coefficient Map

Figure 17 shows the film heat transfer coefficient corresponding to the flow configuration and simulation parameters of Fig. 16. Values shown in Fig. 17 are the h -values in units of $W/m^2 \cdot K$ and temperatures ($^{\circ}C$) for various locations on the MMRTG/HXCH assembly. Having established a baseline simulation, a trade space was identified whereby various windbreaker configuration were to be analyzed using CFD. The trade matrix of various geometric configurations for the windbreaker location are shown below in Fig. 18. The figure shows a tabulation of the CFD Simulation Case (first column), the average heat transfer coefficient on the MMRTG, the hot plate (HP) and the cold plate (CP) of the heat exchanger (column 2), the largest temperature on the MMRTG for CFD versus EES (EES is the acronym for the Engineering Equation Solver simple resistance network of the MMRTG/HXCH thermal model prepared in house at JPL) (third column), and finally the CFD predictions for various temperatures in the MMRTG/HXCH hardware, the inlet, the wake, the cold plate (CP) for CFD versus the EES model, as indicated (fourth column).

	CFD SIMULATION CASE	Ave Conv Coef, $W/m^2 \cdot K$	T_{RTG} ($^{\circ}C$)	T_{HX} ($^{\circ}C$)
1		1.85 RTG 1.1 HP 3.26 CP	104 CFD 109 EES	-51 INLET / -16 WAKE CFD -92 CP, -32 HP EES
2		2.21 RTG 1.49 HP 1.28 CP	72 CFD 99 EES	-108 CFD -82 CP, -52 HP EES
3		1.75 RTG 0.9 HP 1.58 CP	101 CFD 113 EES	-82 CP / -79 HP CFD -79 CP / -25 HP EES
4		1.25 RTG 0.19 HP 1.47 CP	120 CFD 129 EES	-40 CFD -67 CP / -4 HP EES
5		1.14 RTG 0.54 HP 1.26 CP	129 CFD 132 EES	-25 CFD -66 CP / -6 HP EES
6		0.94 RTG 0.24 HP 1.79 CP	133 CFD 139 EES	-28 CFD -68 CP / 2 HP EES

Figure 18. MMRTG/HXCH Windbreaker Location CFD Model Trade Study (HP = hot plate, CP = cold plate, EES = Engineering Equation Solver simple network model)

For instance, the CFD set-up for Case 6 is shown in Fig. 19. Note that when setting up Case 6, the obvious symmetry was employed in order to reduce the overall size of the CFD mesh, and thus to enhance the turn-around time of the simulation.

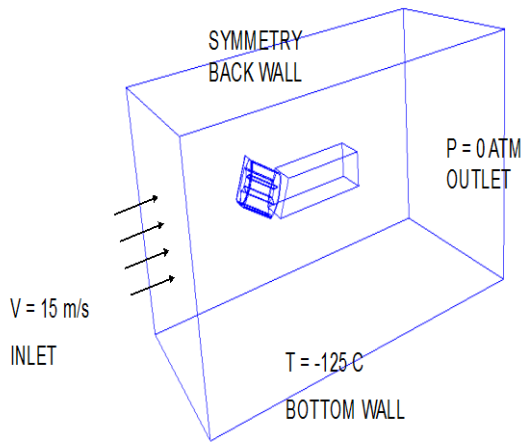


Figure 19. MMRTG/HXCH Windbreaker Location CFD Model Trade Study

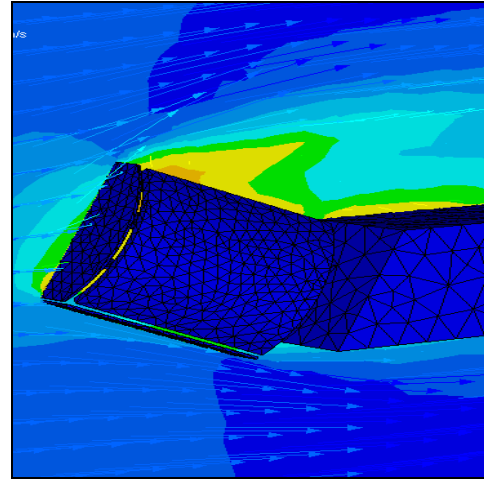


Figure 20. MMRTG/HXCH Windbreaker Case 6: Parallel Flow, Frontal Windbreaker Between Shields and Lower MMRTG Windbreaker

Post processing of Case 6 is included in order to illustrate the agreement of the CFD simulations with simple heat transfer textbook theory. Figure 20 shows the velocity field for the Case 6 simulation. The scale on the color bar ranges from 0 = blue to 19.3 m/s = red. The physical action of the windbreaker on the flow field in the neighborhood of the MMRTG is shown to tailor the flow field such that the predominant wind direction (left to right) is deflected to the top of the MMRTG, and the ensuing flow streamlines around the rover Warm Electronics Box (WEB).

When comparing the CFD results of Case 6 to simple textbook theory, on the outer HXCH the surface can be modeled as flat plate in parallel flow, using the fluid temperature of 196 K, local velocity of $\text{CO}_2 = 15 \text{ m/s}$, length of the plate = 0.65 m. A Reynolds number of 2.9×10^4 was computed, which is less than the critical value of 5×10^5 for flat plate flow, thus the Nusselt number per Eq. (1) below is computed to be $\overline{Nu}_L = 100$.

$$\overline{Nu}_L = 0.664 \sqrt{Re_L} Pr^{1/3} \quad (1)$$

This leads to a heat transfer coefficient of $\overline{h} = 1.4 \text{ W/m}^2\text{-K}$. Post-processing the CFD data leads to $\overline{h}_{CFD} = 1.8 \text{ W/m}^2\text{-K}$. Thus we incur an error of roughly 29%, which is the bias of conservatism, since the CFD predicts more heat transfer than theory does. Also, the 20% error is within the realm of uncertainty of 25% to 30% typically assigned to textbook correlations such as those used in Eq. (1). Finally, for Case 6, from the CFD we find the average temperature on the MMRTG = 406.15 K, the average temperature on the hot HXCH = 245.15 K, and the average temperature on the cold HXCH = 245.15 K (the latter two values due to the symmetry of the flow). Figure 21 shows the heat transfer coefficients ($\text{W/m}^2\text{-K}$) and temperatures (K) at strategic spatial locations within the MMRTG/HXCH assembly.

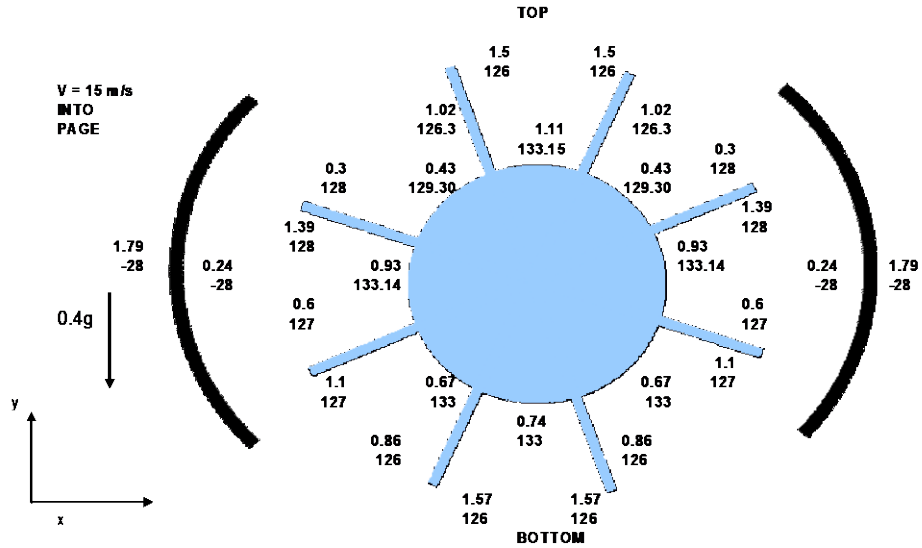


Figure 21. Post-Processing MMRTG/HXCH in Heat Transfer Coefficient Map for Case 6 (values Heat Transfer Coefficient [$\text{W}/\text{m}^2\text{-K}$] / T (K) shown)

The flight design configuration corresponds to Case 4 of Fig. 18, thus it is warranted to summarize the CFD analysis with respect to this simulation case. Figure 22 shows temperature contours for Case 4. The color bar for temperature contours vary from a low of 188.15 K = blue to a high of 456.7 K = red. Case 4 is the configuration whereby the windbreaker is placed to bridge the heat shields, and no windbreaker is installed below the MMRTG.

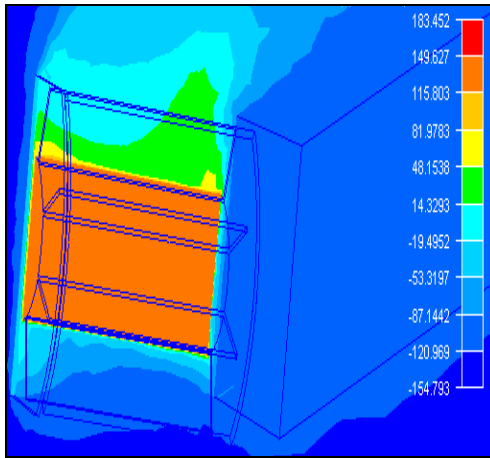


Figure 22. Post-Processing MMRTG/HXCH in Heat Transfer Coefficient Map for Case 4: Parallel Flow, Frontal Windbreaker Between Shields

The buoyant plume arising from the hot surface of the MMRTG (which is at approximately $150^\circ\text{C} = 302^\circ\text{F}$) is apparent from the CFD simulation. Also apparent in Figure 22 is the thermal boundary layer, which sets itself up on the windbreaker. Simulation results of the CFD show the average temperature of the MMRTG = 393.15 K, the average HXCH temperature = 233.15 K, and the average screen temperature = 246.15 K. The heat transfer coefficient map is shown below in Figure 23 below.

CASE 4 RTG AND HEAT EXCHANGERS IN PARALLEL FLOW, SHIELD OVER INLET OF RTG AND HX ONLY
NOTE: h (W/m²-K) / T (°C)

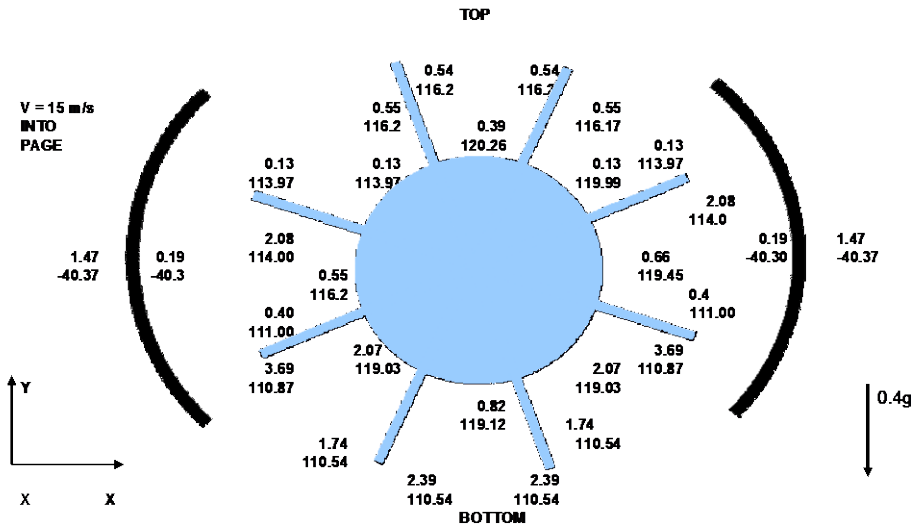


Figure 23. Post-Processing MMRTG/HXCH in Heat Transfer Coefficient Map for Case 4

From the above discussion regarding the CFD analysis, it has been shown how the results of complicated 3-d geometrically coupled heat transfer/fluid mechanics computer software simulations can be efficiently reduced to aid in the guide of design of a thermal control system. In closing, it should be mentioned that verification and validation in the form of simple test cases should always be performed when dealing with any real-world problem, for it is this process which allows the practicing engineer to place an effective error bounds on the results of complex numerical predictions as opposed to textbook correlations. It should be mentioned that the cumulative effects of spatial discretization, employed numerical algorithm, and the NIST thermal properties used for the analysis could add up to as much as 20% error on the CFD results. The only way to ascertain this exactly would be to perform a detailed CFD model correlation using on-station test data. This of course is beyond the scope of the current investigation.

VI. Tradeoff of the WCH/WCC Thermal Performance of the Rover due to the Windbreaker

While it is evident that the windbreaker greatly helps in the conservation of heat in the cold cases in the presence of wind, it does also partially block the MMRTG's view of the environment (sky & ground), which leads to a slight increase in the MMRTG's temperature (when compared to the absence of the windbreaker). The increase in the MMRTG's temperature also leads to an increase in the heat pick up in the hot plate, which then has to be rejected in the radiators. Not all of this excess heat is successfully rejected due to the finite size of the radiators, which then leads to increase in the rover RAMP's temperature.

A thermal analysis of the complete system in the worst-case hot condition showed that the windbreaker led to a relatively small (5°C) increase in the MMRTG's skin temperature and an insignificant (<1°C) increase in the RAMP temperature (the MMRTG's view is blocked by about 5% in the axial direction). Comparison of these slight temperature increases in the WCH conditions to the enormous increase in the WCC conditions of ~30°C in the RAMP temperature clearly exhibits the enormous leveraging in the improvement in the cold conditions when compared to the worsening temperatures in the hot conditions. Thus the windbreaker was a very attractive improvement of the rover thermal design.

VII. Conclusion

This paper presented an overview of the requirements, design and analysis of the effects of wind on the thermal performance of the Mars Curiosity Rover that is currently on Mars. In particular it describes its thermal effect on the MMRTG and its heat exchangers. It describes in detail the analysis of the windbreaker that was an integral part of the design to mitigate the deleterious effects of wind on the rover's thermal performance. CFD analysis was employed to make these assessments. The results show that the windbreaker provided tremendous robustness for the thermal design of the rover in cold conditions without significantly sacrificing its performance in the hot conditions. Overcoming the deleterious effects of the wind was a major challenge, and the simple windbreaker design met the challenge exceptionally well and it was relatively easy to implement. Employment of this

windbreaker as well as the sophisticated CFD analysis used for MSL paved the way for their use in future interplanetary missions in their current or extrapolated forms.

Acknowledgments

The work described in this paper was performed at the Jet Propulsion Laboratory, California Institute of Technology, under a contract with the National Aeronautics and Space Administration. The authors wish to acknowledge the many engineers and scientists collaboratively working on the Mars Science Laboratory project, of which the thermal subsystem is a part of the greater whole.

References

- ¹Bhandari, P., Birur, G.C., and Gram, M.B., "Mechanical Pumped Cooling Loop for Spacecraft Thermal Control," SAE Technical Paper No. 961488, 26th International Conference on Environmental Systems, Monterey, California, July 8-11, 1996.
- ²Birur, G.C., Bhandari, P., Gram, M.B., and Durkee, J., "Integrated Pump Assembly- An Active Cooling System for Mars Pathfinder Thermal Control," SAE Technical Paper No. 961489, 26th International Conference on Environmental Systems, Monterey, California, July 8-11, 1996.
- ³Birur, G. and P. Bhandari, "Mars Pathfinder Active Thermal Control System: Ground and Flight Performance of a Mechanically Pumped Loop," Paper No AIAA-97-2469, 32nd Thermophysics Conference, Atlanta, GA, June 23-25, 1997.
- ⁴Birur, G.C. and Bhandari, P., "Mars Pathfinder Active Heat Rejection System: Successful Flight Demonstration of a Mechanically Pumped Cooling Loop," SAE Technical Paper No. 981684, 28th international Conference on Environmental Systems, Danvers, Massachusetts, July 13-16, 1998.
- ⁵Lam, L, Birur, G., and Bhandari, P., "Pumped Fluid Loops," *Satellite Thermal Control Handbook (2nd edition)*, Ed. D. Gilmore, Aerospace Corporation, El Segundo, California, 2002.
- ⁶Ganapathi, G., Birur, G., Tsuyuki, G., and Krylo, R., "Active Heat Rejection System on Mars Exploration Rover – Design Changes from Mars Pathfinder", Space Technology Applications International Forum 2003, Albuquerque, NM, February 2-5, 2003.
- ⁷Tsuyuki, G., Ganapathi, G., Bame, D., Patzold, J., Fisher, R., and Theriault, L., "The Hardware Challenges for the Mars Exploration Rover Heat Rejection System," AIP Conference Proceedings, Vol. 699(1), pp. 59-70. February 2004.
- ⁸Bhandari, P., "Mechanically Pumped Fluid Loops for Spacecraft Thermal Control, Past, Present and Future", 15th Annual Thermal & Fluid Analysis Workshop (TFAWS), 2004, Pasadena, CA
- ⁹Bhandari, P., Birur, G., Pauken, M., Paris, A., Novak, K., Prina, M., Ramirez, B., and Bame, D., "Mars Science Laboratory Thermal Control Architecture," SAE 2005-01-2828, 35th International Conference on Environmental Systems, Rome, Italy, July 2005.
- ¹⁰Birur, G., Bhandari, P., Prina, M., Bame, D., Yavrouian, A., and Plett, G., "Mechanically Pumped Fluid Loop Technologies for Thermal Control of Future Mars Rovers," SAE 2006-01-2035, 36th International Conference on Environmental Systems, Norfolk, Virginia, July 2006.
- ¹¹Bhandari, P, et al, "Mars Science Laboratory Rover Thermal Control Using a Mechanically Pumped Fluid Loop", Space Technology & Applications International Forum (STAIF-2006), March, 2006
- ¹²Bhandari, P., Birur, G.C., et al, "Mechanically Pumped Fluid Loop Heat Rejection & Recovery Systems For Thermal Control on Martian Surface – Case Study of The Mars Science Laboratory," 36th International Conference on Environmental Systems, Norfolk, Virginia, July 2006.
- ¹³Bhandari, P., Birur, G et al., "Mars Science Laboratory Mechanically Pumped Fluid Loop for Thermal Control – Design, Implementation, and Testing," Paper 2009-01-2437, 39th International Conference on Environmental Systems, Savannah, Georgia, July 2009
- ¹⁴Mastropietro, A.J., Beatty, J., Kelly, F., Birur, G., Bhandari, P., Pauken, M., Illsley, P., Liu, Y., Bame, D., and Miller, J., "Design and Preliminary Thermal Performance of the Mars Science Laboratory Rover Heat Exchangers," Paper AIAA2010-61945 40th International Conference on Environmental Systems, Barcelona, Spain, July 2010
- ¹⁵Birur, G., Bhandari, P., Bame, D., Karlmann, P., Mastropietro, A.J., Liu, Y.M., Miller, J., Pauken, M., and Lyra, J. "From Concept to Flight: An Active Fluid Loop Based Thermal Control System for Mars Science Laboratory Rover," 42nd International Conference on Environmental Systems, San Diego, CA, July 2012
- ¹⁶Incropera, F.P., and Dewitt, D.P., *Introduction to Heat Transfer*, 2nd ed., Wiley, New York, 1990, Chap. 7, pp. 382.
- ¹⁷Patankar, S.P., *Numerical Heat Transfer and Fluid Flow*, Taylor and Francis, 1990, Washington D.C., Chap. 6.
- ¹⁸Anderson, K., Zayas, D. and Turner, D., "CFD Analysis of OPALS Sealed Enclosure Electroincs Subsystem", *Thermal and Fluids Analysis Workshop TFAWS2012*, NASA-JPL, Pasadena, CA, August, 2012.
- ¹⁹NIST12 Standard Reference Database 12, Version 5.0, Boulder, CO, 2004.